UMC Utrecht Universiteit Utrecht

2020
2021

Unravelling the function of circ*Rmst* in the development of midbrain dopaminergic neurons

Author: Lars Michels

Daily supervisor: Mateja Rybiczka-Tesulov

Supervisor: prof. dr. R.J. Pasterkamp

Department: Translational Neuroscience, UMC Utrecht

Abstract

Circular RNAs (circRNAs) are covalently closed non-coding RNA (ncRNA) molecules which are formed by an alternative splicing mechanism called backsplicing. Due to recent improvements in RNA sequencing techniques, circRNAs have been discovered to be widely expressed in a tissue-specific and cell type-specific manner and expression patterns differ throughout embryonic development. Because of the relatively high expression of circRNAs in the developing brain, combined with the fact that many other types of ncRNA play a role in brain development, it is interesting to study the role of circRNAs in this process. Previously in this project, multiple circRNAs specific to midbrain dopaminergic (mDA) neurons in the ventral midbrain (vMB) were found. Among them circular rhabdomyosarcoma 2-associated transcript (circ*Rmst*) was particularly highly expressed in mDA neurons. circ*Rmst* also had a change in expression during development. Therefore, the main aim was to discover the function of circ*Rmst* in the development of mDA neurons. Using lentivirus-delivered short hairpin RNAs (shRNA), circ*Rmst* was knocked down in embryonic vMB primary cultures, which caused an increase in soma size and complexity, and a decreased amount of mDA neurons. *In vivo* knockdown of circ*Rmst*, induced using *in utero* electroporation (IUE), led to altered position of mDA neurons. A function of circ*Rmst* is proposed in which circ*Rmst* could regulate size and migration of mDA neurons by altering the cytoskeleton. Furthermore, circ*Rmst* could be involved in mDA neuron differentiation or survivability. This study provides the first evidence that circ*Rmst* plays a role in mDA neuron development.

Layman's Summary

Dopamine is a neurotransmitter which can modulate neural processes in the mammalian brain. Dopamine is mainly produced in nerve cells in the midbrain, or so called midbrain dopaminergic neurons (mDA neurons). The mDA neurons are responsible for reward, emotional behaviour and decision making, but also motor functions. It is very important that during embryonic development of mDA neurons everything goes according to plan, because little mistakes can lead to severe developmental disorders. Our DNA holds the code for many genes that are important for this process. Developmental genes are, like any other gene, transcribed into RNA and the RNA is translated into a protein. These proteins regulate for example cell growth or cell migration during development. However, there also some RNAs that are not transcribed into protein, but have a function of their own. One of these RNAs is the circular RNA circ*Rmst*. This study found that circ*Rmst* is located in mDA neurons that are in development. To learn about the function of circ*Rmst*, the circular RNA can be destroyed to see what happens to neurons when circ*Rmst* is not available. This was done firstly in alive developing mouse mDA neurons. This lead to an increase in size and complexity of the mDA neurons. When circ*Rmst* was destroyed in the mouse midbrain, a change in neuron migration was found. This study provides the first evidence that circ*Rmst* plays a role in mDA neuron development.

Table of contents

1. Introduction

1.1 A new class of noncoding RNAs: circular RNAs

In the past, the generally accepted mechanism of gene expression was that genes that are encoded in DNA are transcribed into messenger RNA (mRNA) and translated into a functional protein. However, in more recent years it has become known that at least 98% of the human genome is not translated into protein (Birney et al., 2007). The majority of genes produce non-coding RNA (ncRNA), which by definition do not produce proteins (Elgar and Vavouri, 2008). Many different types of ncRNAs have already been identified with a wide range of functions, including ribosomal RNAs (rRNAs), transfer RNAs (tRNAs), microRNAs (miRNAs) and long non-coding RNAs (lncRNAs) (Ambros, 2004; Burdon, 1971; Cech, 1990; Kruger et al., 1982). Recently, a new class of ncRNAs, circular RNAs (circRNAs), has received a lot of attention.

CircRNAs are formed by a non-canonical splicing mechanism, in which the 3' and 5' splice sites of exons and/or introns of an RNA are covalently linked, forming a circular RNA molecule. This process is called backsplicing. During backsplicing the so-called backsplice junction is formed where the ends of the circularised RNA meet (Chen and Yang, 2015). CircRNAs were first discovered in eukaryotic cell lines by using electron microscopy (Hsu and Coca-Prados, 1979). However, the significance of circRNAs was mostly dismissed in the next decades as they were considered a by-product of pre-mRNA splicing (Cocquerelle et al., 1993). Only the circRNA produced by the sex-determining region Y (*Sry*) gene was predicted to have a function (Capel et al., 1993). Recent advances in RNA-sequencing techniques (RNAseq) and bioinformatics protocols have provided evidence that many genes produce circRNAs and that circRNAs are the predominantly transcribed RNA from certain genes (Salzman et al., 2012; Wang et al., 2014). Moreover, circRNAs are found in a myriad of different eukaryotes, including plants, fungi, worms, fruit flies and mammals (Salzman et al., 2012; Wang et al., 2014). Lastly, circRNAs can be tissue- and cell type-specific with an especially high expression in the brain (Maass et al., 2017; Salzman et al., 2013; Xia et al., 2017).

1.2 Backsplicing and biogenesis of circRNAs

In canonical splicing, a big complex of small nuclear RNAs (snRNAs) and proteins, called the spliceosome removes introns from pre-mRNA to form mature mRNA that usually consists of only exons. Backsplicing makes use of the same splice sites as are used in canonical splicing (Jeck et al., 2013). Mutagenesis analysis in vectors that overexpress circRNAs revealed that the spliceosome is required for backsplicing and that backsplicing competes with canonical splicing of pre-mRNA (Ashwal-Fluss et al., 2014; Starke et al., 2015). However, RNA interference (RNAi) analysis in *Drosophila* cells showed that depletion of certain spliceosomal factors increased backsplicing activity (Liang et al., 2017). This indicates that while the spliceosome is necessary for backsplicing, other mechanisms are also needed to steer canonical splicing towards backsplicing. It is suggested that by slowing down the functionality of the spliceosome, the backsplicing machinery can be directed to more easily transform nascent RNA into circRNA (Liang et al., 2017).

For efficient circularisation, looping of a pre-spliced RNA is required to bring splice sites closer together. Depending on the gene locus, looping can be mediated by multiple separate mechanisms. Some circRNAs are looped by base pairing of inverted complementary repeated sequences such as Alu pairs (Figure 1 (A1); Zhang et al., 2014). These can be present in introns flanking the to be circularized exons. RNA binding proteins (RBPs) FUS and Quaking can also mediate backsplicing by binding to introns flanking the backsplice junction and dimerising (Figure 1 (A2); Conn et al., 2015; Errichelli et al., 2017). Nuclear factor 90 (NF90) and its isoform NF110 bind to intronic RNA pairs, which stabilizes them and promotes circRNA formation during viral infection (Figure 1 (A2); Li et al.,

2017). Contrarily, adenosine deaminase acting on RNA (ADAR1) inhibits backsplicing by binding to intronic RNA pairs and converting adenosine into inosine (Figure 1 (B1); Ivanov et al., 2015). This leads to weaker binding of intronic RNA pairs. Knockdown of ADAR1 in human cells results in increased circRNA expression and overexpression of ADAR1 leads to reduced circRNA expression (Ivanov et al., 2015; Rybak-Wolf et al., 2015). DExH-Box Helicase 9 (DHX9) blocks circularisation of RNA as well by unwinding intronic RNA pairs (Figure 1 (B1); Aktaş et al., 2017; Koh et al., 2014). Together these mechanisms allow the cell to regulate backsplicing dynamically.

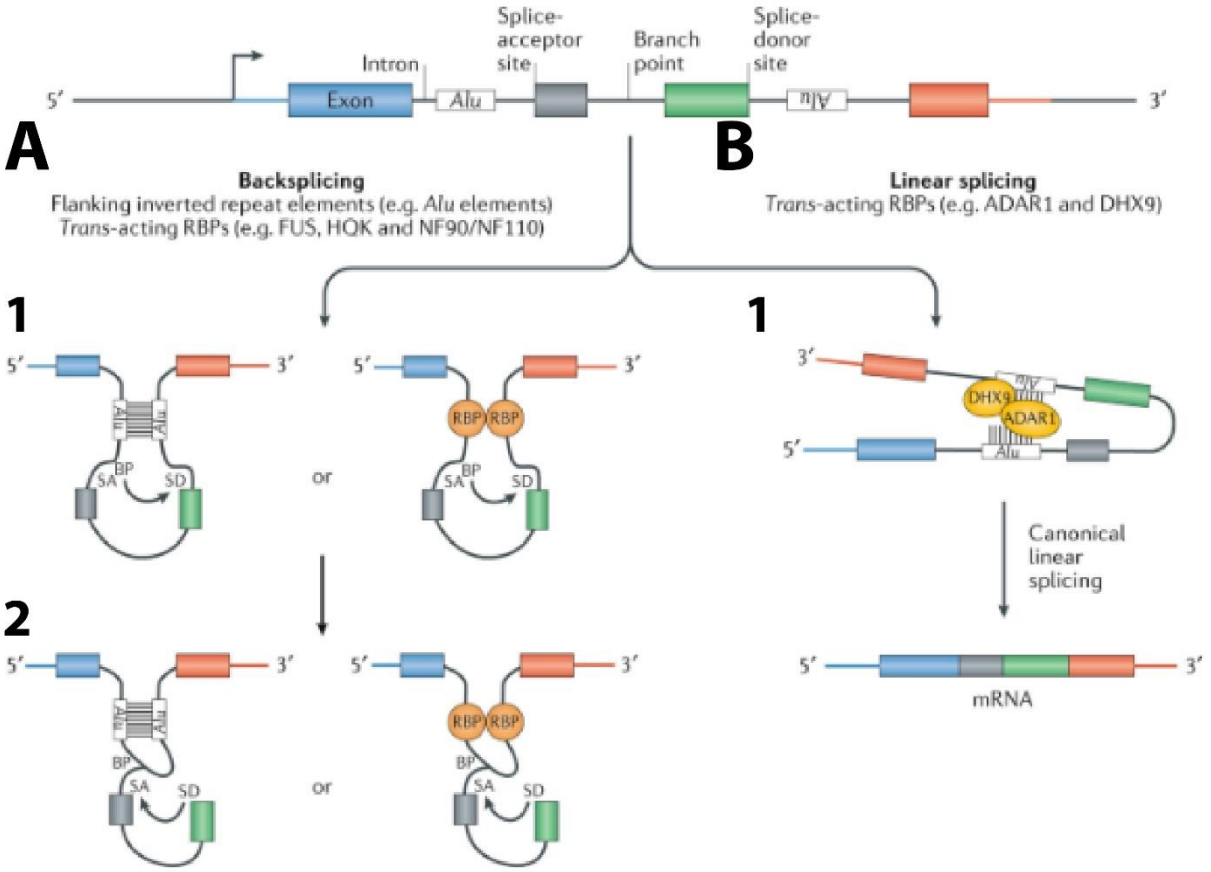

Figure 1. Backsplicing and Linear splicing *Pre-processed RNA consists of exons and introns. CircRNAs are formed when the ends of exons are covalently bound to each other in a process called backsplicing, which forms the backsplice junction. This can be mediated by looping the RNA by pairing of inverted Alu repeats (A1) or dimerization of trans-acting RBPs such as FUS, Quaking (HQK) and NF90/NF110 (A2). Backsplicing can be inhibited by trans-acting RBPs ADAR1 and DHX9 by editing and unwinding RNA respectively, leading to increased canonical linear splicing (B1; Modified from Kristensen et al., 2019).*

1.3 Molecular mechanisms of circRNAs

Since circRNAs are highly and spatiotemporally expressed in many organisms, it has been suggested that circRNAs could play an important role in cellular processes. Indeed, a lot of molecular mechanisms have been discovered in which circRNAs are involved. Some of these mechanisms include acting as a miRNA or protein sponge, acting as a scaffold for RBPs, regulation of transcription and translation of circRNAs.

The first mechanism of circRNAs that was discovered is the ability of some circRNAs to act as a miRNA sponge (Hansen et al., 2013; Memczak et al., 2013). For example, cerebellar degeneration-related protein 1 antisense transcript (CDR1as, also known as ciRS-7) has more than 70 binding sites for miR-7. Human CDR1as expression in zebrafish gives rise to a malformation in the midbrain, which is a similar phenotype to miR-7 knockdown. This indicates that by binding miR-7, CDR1as inhibits miR-7 function (Memczak et al., 2013). This leads to a decrease in targeted mRNA degradation by

miR-7. Another example is the circRNA *Sry* which functions as a sponge for miR-138 (Hansen et al., 2013).

CircRNAs can also function as a protein sponge. The gene *muscleblind* (*mbl*) produces both the splicing factor MBL and circ*Mbl* (Ashwal-Fluss et al., 2014). MBL promotes circularisation of its own gene by binding to the flanking introns of circ*Mbl*, bringing them closer together. Thus, MBL can regulate its own translation by making its own mRNA circular and untranslatable. circ*Mbl* has many binding sites for MBL and acts as a sponge, further decreasing MBL activity.

The expression of circular Forkhead box O3 (circ*Foxo3*) is correlated with the cell cycle of mouse fibroblasts (Du et al., 2016). In these cells circ*Foxo3* acts a scaffold for two proteins which makes them able to interact more easily. circ*Foxo3* binds to both p21 and cyclin-dependent kinase 2 (CDK2). This provides access for p21 to bind to and inhibit CDK2, halting the cell cycle (Du et al., 2016). Another protein scaffolding circRNA is circular Angiomotin Like 1 (circ*Amotl1*), which is highly expressed in human neonatal cardiac tissue (Zeng et al., 2017). circ*Amotl1* can bind to Pyruvate Dehydrogenase Kinase 1 (PDK1) and AKT1, resulting in phosphorylation of AKT1 by PDK1 (Zeng et al., 2017).

Some circRNAs are able to regulate transcription as well. Exon-intron circRNAs (EIciRNAs) are a category of circRNAs that consist of both exons and introns and interact with U1 small nuclear ribonucleoprotein (U1 snRNP; Li et al., 2015). These EIciRNAs use this RNA-RNA interaction to further enhance their own transcription via the RNA-polymerase II transcription complex.

A few circRNAs that can be translated into peptides have been identified. circ*Mbl* undergoes cap-independent translation, making use of internal ribosome entry sites (IRESs) and a stop codon (Pamudurti et al., 2017). This translation produces small peptides that are distinct from the proteins produced by mRNA from the same gene. The peptides are predicted to have a function in synapses, because of their presence in synaptosomes (Pamudurti et al., 2017). However, the exact function of these peptides has not been discovered yet.

1.4 Development of dopaminergic midbrain neurons

The majority of dopaminergic (DA) neurons in the brain are found in the ventral midbrain. These dopaminergic neurons of the midbrain (mDA neurons) are organised in three different subgroups, the retrorubral field (RrF or A8), the substantia nigra pars compacta (SNc or A9) and the ventral tegmental area (VTA or A10; Arenas et al., 2015). These subgroups have distinct projections and functions. The VTA and RrF innervate the ventral striatum (nucleus accumbens), parts of the limbic system and the prefrontal cortex (PFC; Tzschentke and Schmidt, 2000). This so-called mesocorticolimbic system is responsible for reward, emotional behaviour and decision making. The SNc innervates the dorsal striatum forming the nigrostriatal pathway, which is responsible for motor function and degenerates in Parkinson's disease (Toulouse and Sullivan, 2008).

During embryonic development, many transcription factors and growth factors are needed to correctly form the mDA neurons in the ventral midbrain. First, the region called the isthmic organiser (IsO) forms the midbrain-hindbrain border by regulating the expression of transcription factors orthodenticle homolog 2 (Otx2) and gastrulation brain homeobox 2 (Gbx) in the midbrain and hindbrain respectively (Rhinn and Brand, 2001). Signals from the IsO and the notochord lead to the origination of mDA neuron progenitor cells in the floorplate of the neural tube (Ono et al., 2007). LIM homeobox transcription factor a (Lmx1a), Lmx1b and Wingless-related integration site 1 (Wnt1) are essential for the specification of mDA neuron progenitor cells (Brown et al., 2011, p. 1; Deng et al., 2011; Smidt et al., 2000). Upregulation of these genes leads to expression of nuclear receptor 4a2 (Nurr1) and pituitary homeobox 3 (Pitx3) which are important for differentiation and survival of mDA

neurons (Chung et al., 2009). Nurr1 and Pitx3 will in turn cause expression of tyrosine hydroxylase (TH), which is the rate-limiting enzyme for dopamine production (Saucedo-Cardenas et al., 1998). This causes these cells to become mature mDA neurons.

1.5 Potential role for circ*Rmst* in mDA neurons

This short introduction on the development of mDA neurons does not cover the full complexity of the biological machinery. There is a plethora of other molecules that play a role in building the dopaminergic system. There are indications that even circRNAs may have functions on the development of mDA neurons. Firstly, circRNAs are especially highly expressed in the brain and expression happens in a spatiotemporal manner (Maass et al., 2017; Rybak-Wolf et al., 2015; Venø et al., 2015; Xia et al., 2017). It was found that in porcine brain development the expression of thousands of circRNAs was differentially regulated in different brain regions over time (Venø et al., 2015). Furthermore, circRNA isotypes of the same gene could be differentially expressed as well (Venø et al., 2015). Another study showed that from a selection of circRNAs that were expressed in the brain, many were highly expressed in the midbrain (Rybak-Wolf et al., 2015). As mentioned earlier, CDR1as overexpression in zebrafish lead to malformations of the midbrain, which is the first time a circRNA has been found to have a function in midbrain development (Memczak et al., 2013).

Lastly, there are many other types of ncRNAs that are important for mDA neuron development (reviewed by Pascale et al., 2020). An important example is the lncRNA rhabdomyosarcoma 2-associated transcript (*Rmst*) as it is a marker for mDA neurons in the ventral midbrain during development (Uhde et al., 2010). *Rmst* is particularly interesting, because the predominant isoform of the transcript in humans is the circRNA circ*Rmst* (Izuogu et al., 2018). *Rmst* has already been found to play a role in neurogenesis by directly binding to Sox2 (Ng et al., 2013). *Rmst* is required for Sox2 to bind to promoter regions of neurogenic transcription factors. Furthermore, *Rmst* and miR135a2, which are expressed from the same gene, are involved in mDA neuron defining pathways together with Lmx1b and Wnt1 (Anderegg et al., 2013). Lmx1b either indirectly or directly upregulates expression of *Rmst* and miR135a2, which in turn repress Lmx1b and Wnt1 signalling. Lastly, *Rmst* can induce apoptosis by directly binding heterogeneous nuclear ribonucleoprotein K (hnRNPK) and activating the p53/miR-107 pathway (Cheng et al., 2020). As the presence of circ*Rmst* was largely unknown or disregarded in the beforementioned studies, circ*Rmst* could be involved in the discovered molecular mechanisms of *Rmst* as well. Therefore, it is hypothesised here that circ*Rmst* plays a role in mDA neuron development.

Previously in this project, RNAseq data of developing mouse mDA neurons were analysed. It was found that several circRNAs were specific to mDA neurons (unpublished data). circ*Rmst* was particularly interesting as it showed a high circular to linear RNA ratio and a change in expression during development (unpublished data). The main aim of the project was to unravel the function of circ*Rmst* in the development of the mDA system. Using a lentivirus-delivered short-hairpin RNA (shRNA) against circ*Rmst*, we showed that depletion of circ*Rmst* causes an increase in soma size and neuron complexity of mDA neurons and a reduction of TH-positive neurons in embryonic primary cultures of the ventral midbrain. *In utero* electroporation (IUE) of a plasmid containing a shRNA against circ*Rmst* was performed on embryonic mouse brains. This lead to a positional defect of mDA neurons. However, the mDA neuron soma size increase cannot be found *in vivo*. The results show that circ*Rmst* is involved in mDA neuron development.

2. Experimental procedures

2.1 Animals

C57BL/6 (wildtype (WT)) mice were used for ventral midbrain (vMB) primary cultures. Heterozygous *Pitx3*$^{Cre/WT}$ mice were used for IUEs (Smidt et al., 2012). *Pitx3Flp:CCK-Cre:Ai65* mice were used for whole tissue clearing (Madisen et al., 2015; Taniguchi et al., 2011). All mouse use was in accordance with local institution guidelines of the University Medical Center Utrecht (UMCU) and approved by the Dierexperimenten Ethische Commissie Utrecht. Mice were kept at a controlled 12h day/night-cycle at a mean temperature of 22°C with radio turned on. Mice were kept in a cage layered with woodchips and enriched with tissues, and had *ad libitum* access to food and water.

2.2 Primary culture from mouse vMB

Round 12 mm coverslips were sterilized by first washing them in 70% ethanol with dH_2O, then 100% ethanol, after which they were shortly flamed to dry. Next, they were incubated in 50 μg/mL Poly-L-Ornithine (Sigma-Aldrich) for 1 hour at 37°C or overnight at 4°C. Coverslips were washed 3 times with dH_2O, after which they were dried, placed in a 24-wells plate and sterilized with UV for 20 minutes. Coverslips were incubated in 10 μg/mL Laminin (Sigma-Aldrich) in Phosphate Buffered Saline (PBS) for 2 hours at 37°C, after which they are washed twice with PBS.

vMBs of embryonic day (E)14 WT were dissected on ice in medium A (10x Hank's Balanced Salt Solustion (HBSS) -$MgCl_2$ -$CaCl_2$ (Gibco), 7% Trehalose (MP Biomedicals), 16 mM HEPES (Gibco)). Tissue was dissociated for 20 minutes at 37°C using Papain and DNase dissolved in papain solution (24 U/ml papain (Worthington Biochemical Corporation), 120 U/mL DNase I (Worthington Biochemical Corporation), 1x HBSS -MgCl2 -CaCl2, -$NaHCO_3$ (Gibco), 1.12% $NaHCO_3$ (Gibco), 50 U/mL Penicillin and 50 μg/mL Streptomycin (P/S; Gibco), 1mM Sodium Pyruvate (Gibco), 0.6% Trehalose, dissolved in dH_2O). Supernatant was aspirated and cells were washed with 5 mL Trituration solution (2.4 U/mL DNase I, 0.2% Bovine Serum Albumin (BSA; Sigma-Aldrich), 4.76% Trehalose, 0.15 mM Sodium Pyruvate, 7.6 U/ml Penicillin, and 7.6 μg/ml Streptomycin in Neurobasal medium (Gibco)) to stop papain digestion. Cells were mechanically dissociated with three fire polished Pasteur pipettes with decreasing diameter in Trituration solution. Cells were purified by transferring them onto BSA column solution (2.2 U/mL DNase, 0.34% BSA, 4.36% Trehalose, 0.14 mM Sodium Pyruvate, 6.9 U/mL Penicillin, 6.9 μg/mL Streptomycin, 2.8 mM NaOH (Merck Millipore) in Neurobasal medium) and centrifugation at 200 g for 4 minutes. Supernatant was aspirated, before adding 800 μL Complete growth medium (54 U/ml Penicillin, and 54 μg/ml Streptomycin, 0.54 mM Glutamax (Gibco), 1.1x B27 plus Supplement (Gibco), 3.6 mM D-Glucose (Sigma-Aldrich) in Neurobasal Plus medium (Gibco)) to the cell pellet. Cells were counted using Countess II FL Automated Cell Counter (Invitrogen). 120000 cells were plated in a drop on each coverslip. After 60 minutes of incubation (37°C at 5% CO_2), wells were filled up to 400 μL with Complete growth medium.

2.3 Transformation and plasmid preparation circ*Rmst* KD plasmids

For amplification of pLentiLox3.7 (pLL3.7) lentiviral vector (Addgene) cloned with an shRNA targeting circ*Rmst* or a scrambled sequence (Scr2), 10 pg to 100 ng of pLL3.7shcirc*Rmst* or pLL3.7Scr2 was pipetted on top of frozen, chemically competent *E. coli* (One Shot Stbl3; Invitrogen), after which they were thawed on ice for 30 minutes. Thereafter, cells were heat-shocked for 45 seconds at 42°C and placed on ice for 2 minutes. 250 μL of room temperature (RT) S.O.C. medium (One Shot) was added and cells are shaken for 1 hour at 37°C at 170 RPM (Eppendorf Innova 43). Cells were spread on a selective 1.5% agar (BD), 2.5% LB (BD) plate with 50 μg/mL Ampicillin (Sigma-Aldrich) and incubated overnight at 37°C. Colonies were collected with a pipette tip and incubated while shaking in 3 mL 2.5% LB in H_2O with 50 μg/mL Ampicillin throughout the day at 37°C. The cell culture was then added to 250 mL 2.5% LB in H_2O with 50 μg/mL Ampicillin for overnight culturing while shaking at 37°C.

Plasmid preparation was performed with the LabNed Plasmid Maxiprep Kit (LN2400007) according to manufacturer's protocol. Plasmid concentration was measured using a Varioskan LUX (Thermo Scientific). Plasmids were stored at -20°C until use.

2.4 HEK 293T culture for lentivirus production

For lentivirus production, Human Embryonic Kidney 293T cells (HEK 293T) were cultured in growth medium (DMEM high glucose medium (Gibco), 10% Foetal Bovine Serum (FBS; Biowest), 1% Penicillin-Streptomycin) at 37°C at 5% CO_2. Cells were split twice a week. For splitting, cells were washed twice with prewarmed 1x PBS, after which they were incubated in 0.25% trypsin (Biowest) and 0.01 mM EDTA in 1x PBS for up to 5 minutes. Growth medium was added and dissociated cells were collected and centrifuged for 4 minutes at 4°C at 1000 g. The pellet was resuspended in growth medium and plated 1:10 in a new flask in fresh medium.

2.5 Lentivirus production

Lentiviruses expressing pLL3.7shcirc*Rmst* and pLL3.7Scr2 were produced in HEK 293T cells in the Pasterkamp laboratory.

2.6 circ*Rmst* knockdown induction using a lentivirus containing shRNA con

vMB primary cultures were infected with lentivirus with pLL3.7shcirc*Rmst* and pLL3.7Scr2 constructs to knock down circ*Rmst* or act as a control respectively. Infections were carried out by colleagues of the Pasterkamp lab. Knockdowns were confirmed by RT-qPCR targeting the backsplice junction to test if circ*Rmst* knockdown was efficient.

2.7 Immunocytochemistry of vMB primary cultures

E14 DIV3 vMB primary culture were fixed with 4% Paraformaldehyde (PFA; VWR) in 1x PBS for 15 minutes at RT, after which they were washed three times with PBS and incubated in blocking buffer (1% BSA and 0.4% Triton-X100 (Roche) in PBS) at RT in a humidified incubation chamber. After blocking, cells were incubated in primary antibodies (1:500 Chicken anti-GFP (AVES, AB_2307313), 1:500 Rabbit anti-TH (Millipore, AB_152)) in 70 µL blocking buffer overnight at 4°C. Cells are washed three times with PBS for 30 minutes and incubated for 2 hours at RT with secondary antibodies dissolved in blocking buffer (1:500 Donkey anti-Chicken Alexa Fluor 488 (Jackson ImmunoResearch, 703-545-155), 1:500 Donkey anti-Rabbit Alexa Fluor 568 (Abcam, AB_175470)). Cells were washed twice with PBS, followed by incubation in 2-(4-Amidinophenyl)-6-indolecarbamidine dihydrochloride (DAPI; Sigma-Aldrich) for 20 minutes at RT. Cells are then washed once more with PBS, dipped in H_2O, dried shortly and mounted on microscopy slides in Mowiol (Sigma-Aldrich). Mowiol was left to dry overnight at RT and samples were stored at 4°C.

Images were taken on an epifluorescence microscope (Zeiss; Axio Scope A1) at 10x and 20x magnification.

2.8 Immunohistochemistry of *in utero* electroporated mouse brains

At E12 *in utero* electroporated *Pitx3*$^{Cre/WT}$ mouse brains were collected at E18 on ice in PBS and fixed overnight in 4% PFA at 4°C. Brains were washed three times in PBS and embedded in 4% low-melting agarose (Invitrogen) in H_2O. They were cut into 60 µm thick free-floating sections on a vibratome (Leica VT1000S) in PBS. Sections were incubated in blocking buffer (10% FBS and 1% Triton-X100 in PBS) for 2 hours on an orbital shaker. Sections were incubated in primary antibody (1:500 Chicken anti-GFP (AVES, AB_2307313), 1:500 Rabbit anti-RFP (Rockland, 600-401-379), 1:500 Sheep anti-Th (Pel-Freez, P60101-150)) in blocking buffer overnight at 4°C. Next day, sections were washed in PBS three times for 30 minutes and incubated in secondary antibody (1:500 Donkey anti-Chicken Alexa

Fluor 488 (Jackson ImmunoResearch, 703-545-155), 1:500 Donkey anti-Rabbit Alexa Fluor 568 (Abcam, AB_175470), Donkey anti-Sheep Alexa Fluor 647 (Abcam, AB150179)) in blocking buffer for 2 hours at RT on an orbital shaker. Slices were washed twice with PBS, followed by 20 minutes staining with DAPI on an orbital shaker. Slices were then washed once more and mounted from PBS with 2% gelatine (Sigma-Aldrich) on microscopy slides and covered with Mowiol and a glass coverslip. Mowiol was left to dry overnight at RT after which samples were kept in the dark at 4°C.

Images were taken on a confocal microscope (Zeiss LSM880 AxioObserver Z1)

2.9 Immunohistochemistry 3Disco and iDISCO clearing of whole brain

Pitx3Flp:CCK-Cre:Ai65 embryos were sacrificed, brains were dissected on ice and meninges were taken off. Brains were fixed in 4% PFA overnight at 4°C and washed three times in PBS. Samples were incubated in PBS with 0.2% gelatine, 0.5% TritonX100 (PBSGT) and 1mg/mL saponin (Sigma-Aldrich) in a rotating rack for 1-4 days at RT. Then, samples were incubated in primary antibody (1:500 Sheep anti-Th (Pel-Freez, P60101-150), 1:500 Rabbit anti-RFP (Rockland, 600-401-379)) diluted in blocking buffer (10% FBS and 1% Triton-X100 in PBS) in a shaking incubator for 1 week at 37°C. Samples were rinsed in PBSGT without saponin 6 times during one day at RT in a rotating rack. Samples were incubated with filtered (0.22 μm filter) secondary antibody (1:500 Donkey anti-Rabbit Alexa Fluor 647 (Invitrogen, A-31573), 1:500 Donkey anti-Sheep Alexa Fluor 750 (Abcam, AB_175756)) in PBSGT with 1mg/mL saponin in a shaking incubator for 3 days at 37°C. Samples were again rinsed in PBSGT without saponin 6 times during one day at RT in a rotating rack.

For 3DISCO clearing (Ertürk et al., 2012), samples were incubated on a rotating rack at RT consecutively in 50% Tetrahydrofuran (THF; Sigma-Aldrich) in H_2O overnight, 80% THF for 1 hour, 100% for 1 hour and 100% for 1 hour again. Samples were transferred to 100% Dichloromethane (DCM; Sigma-Aldrich) for 30 minutes or until brains sunk. Samples were then transferred to 100% Benzyl ether (DBE; Sigma-Aldrich) and left for a few hours until transparent. Samples were kept in the dark at RT until imaging.

For iDISCO clearing (Renier et al., 2014), samples were incubated on a rotating rack at RT consecutively in 20% Methanol (VWR) in PBS, 40% Methanol, 60% Methanol, 80% Methanol, 100% Methanol and 100% Methanol for 1 hour each, after which samples were incubated in 66% DCM and 33% Methanol overnight at RT. Samples were then washed in DCM for 30 minutes after which they were transferred to DBE and left for a few hours until transparent. Samples were kept in the dark at RT until imaging.

Samples were imaged on a light sheet microscope (Olympus MVX10). Images were visualised and analysed in Imaris.

2.10 Soma size analysis primary vMB culture

Coverslips with primary vMB cultures were imaged on an epifluorescence microscope (Zeiss; Axio Scope A1) at a magnification of 20x. Pictures were analysed with Fiji (v1.53c). The scale was first set to 1.960 pixels/micron. '*Freehand Selections*' tool was used to carefully draw a shape along the edge of the soma of a TH-positive and GFP-positive neuron in the TH channel. A shape was also drawn along the edge of the nucleus of the same cell in the DAPI channel. Both regions of interest (ROIs) were measured to determine the surface area (size) [μm^2] of the soma and nucleus. Surface area of TH-positive neurons in the pLL3.7shcirc*Rmst* condition was normalized to the pLL3.7Scr2 condition. An unpaired t-test was performed for soma size and soma size to nucleus size ratio using Graphpad (v8.4.0.671).

2.11 TH-positive cell percentage analysis primary vMB culture

Coverslips with primary vMB cultures were imaged on an epifluorescence microscope (Zeiss; Axio Scope A1) at a magnification of 10x. Pictures were analysed with Fiji. The scale was first set to 0.982 pixels/micron. TH-positive cells were manually counted in the TH channel. Total amount of cells was determined by counting DAPI-stained nuclei. To do this, a gaussian blur was performed on the DAPI channel with a Sigma of 1.5 μm. A default automated threshold was set, followed by a '*Watershed*' mask. Function '*Analyze Particles…*' was then used to count total amount of cells. TH-positive percentage in the pLL3.7shcirc*Rmst* condition was normalized to the pLL3.7Scr2 condition. An unpaired t-test was performed using Graphpad.

2.12 Complexity analysis primary vMB culture

Images with a magnification of 20x from primary vMB culture were qualitatively assessed in Fiji. Soma of neurons were divided into categories 1 to 5, ranging from least complex to most complex and quantified. Category 1: No lamellipodia, smooth soma surface, 2-3 extensions; Category 2: Small lamellipodia, smooth soma surface, 3-4 extensions; Category 3: Medium lamellipodia, mostly smooth soma surface, 4-5 extensions; Category 4: Big lamellipodia, smooth soma surface only on some parts, ≥5 extensions; Category 5: Extensive lamellipodia, no smooth cell body surface, ≥5 extensions.

2.13 Soma size analysis IUE brains

IUE *Pitx3*$^{Cre/WT}$ brain slices were imaged on a confocal microscope (Zeiss LSM880 AxioObserver Z1). Pictures were opened in ImageJ with Fiji extension installed. First a '*Max Intensity*' projection of the Z-stack was made. Using the '*Freehand Selections*' tool, an ROI was drawn around the area which contained TH-positive neurons in the TH channel. A shape was drawn around the somas of TH-positive neurons in this area using the '*Freehand Selections*' tool. ROIs of somas were measured to determine the area [μm^2]. An unpaired t-test was performed using Graphpad.

3. Results

3.1 Knockdown of circ*Rmst* leads to increase of soma size and neuron complexity, and a decrease of TH-positive mDA neurons

Previously in this project, a knockdown of circ*Rmst* was performed in mouse E14 primary cultures of the vMB using a shRNA against circ*Rmst* (pLL3.7shcirc*Rmst*) and an empty vector (pLL3.7GFP) construct was used as a control. This was done to study the function of circ*Rmst* in mDA neurons. Many morphological parameters were analysed, including neurite length, number of branches, soma size and soma size/nucleus size ratio. The percentage of TH-positive cells was also determined. Soma size and soma size/nucleus size ratio were found to be significantly increased and TH-positive percentage was found to be significantly decreased (unpublished data; not shown). However, in the empty vector control no shRNA was produced. This means that there was still an uncertainty that the significant effects from the knockdown could be caused by upregulation of RNAi mechanisms.

Here, a shRNA with a scrambled sequence (Scr2) that did not have any predicted binding partners was used as a control. In lentivirus-infected vMB primary cultures, pLL3.7shcirc*Rmst* TH-positive cells appeared to have an enlarged soma area compared to pLL3.7Scr2 (Figure 2 (A,B)) infected cells. This was quantified and a significant increase in soma size was found in the circ*Rmst* knockdown condition compared to Scr2 control ($p=0.0185$; Figure 2 (C)). To see if the increase in soma size occurred relatively to the nucleus, soma size/nucleus size ratio of TH-positive cells was also calculated. A significant increase in soma size/nucleus size ratio was found as well in the circ*Rmst* knockdown condition ($p= 0.0114$; Figure 2 (D)).

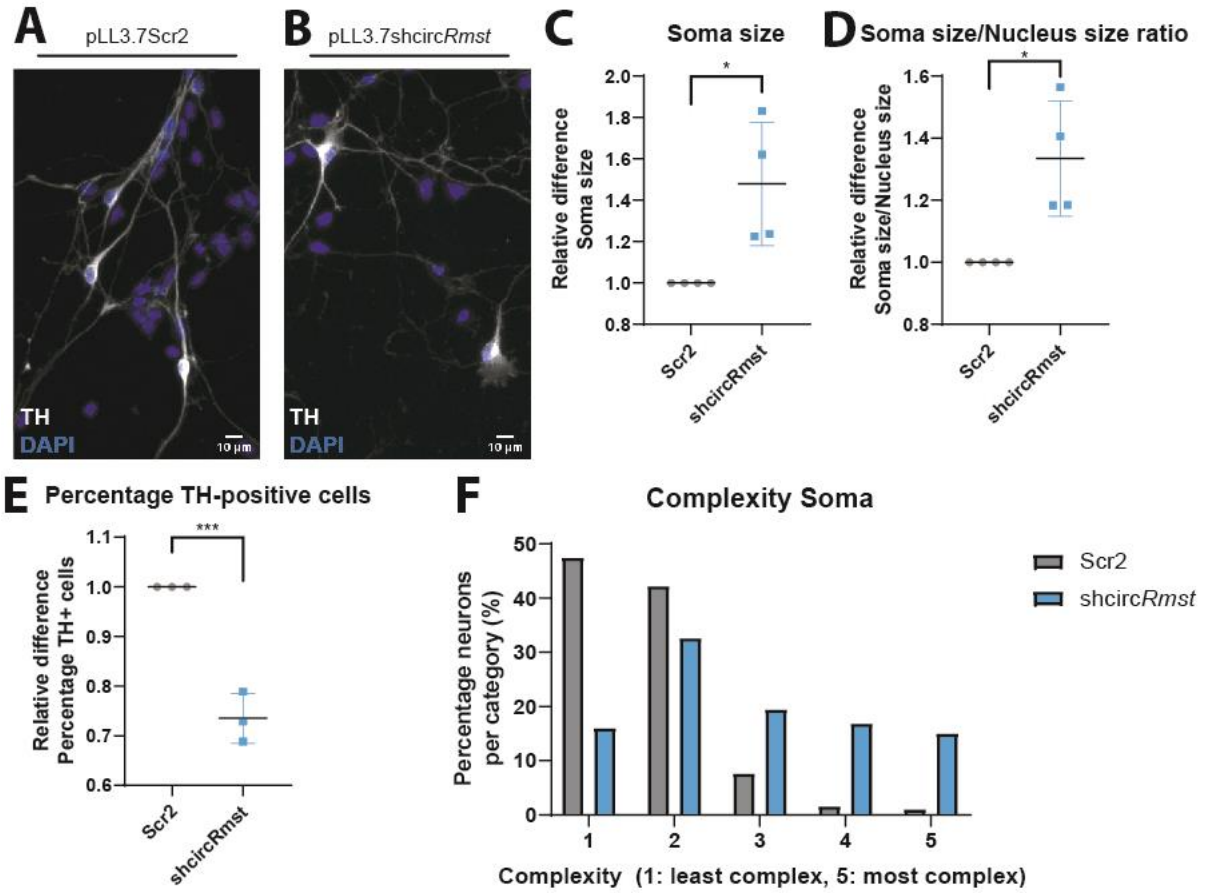

Figure 2. Soma size, soma size/nucleus size ratio, percentage TH-positive neurons and complexity are affected by circRmst knockdown *A,B E14 primary culture of vMB with pLL3.7Scr2 control (A) and pLL3.7shcircRmst knockdown (B), stained with anti-TH antibodies and DAPI (Scalebar 10µm, 20x). Soma size (C), soma size/nucleus size ratio (D) and percentage TH-positive cells (E) were quantified and a relative analysis is performed (bars: mean ± S.E.). Complexity of somas were analysed and divided into 5 categories (F; 1: least complex, 5: most complex). Statistical analysis was performed using the two-way unpaired t-test (C-E; *, p < 0.05; ***, p < 0.001).*

Next, the percentage of TH-positive neurons in infected primary vMB cultures was quantified. Here a significant decrease of TH-positive neuron percentage was found in the circ*Rmst* knockdown condition compared to control (p= 0.0008; Figure 2 (E)).

Lastly, complexity of somas of TH-positive neurons was analysed, to see if somas not only became bigger, but also more complex. Every cell was divided into one of five categories based on complexity of which 1 was the least complex and 5 the most complex. 89% of TH-positive neurons from the pLL3.7Scr2 control cultures fell into the least complex categories 1 and 2, 9% in category 3 and only 2% in categories 4 and 5 (Figure 2 (F)). Of the TH-positive neurons from the pLL3.7shcirc*Rmst* knockdown cultures, only 50% were found in the least complex categories 1 and 2, 17% in category 3 and 32% in the most complex categories 4 and 5, indicating an increase in complexity (Figure 2 (F)). In summary, we find an increase in soma size, soma size/nucleus size ratio, and a decrease in the percentage of TH-positive neurons when circ*Rmst* is knocked down. This suggests a role of circ*Rmst* in mDA neuron development.

3.2 Knockdown of circ*Rmst in vivo* leads to positional defect of mDA neurons

To study whether a knockdown of circ*Rmst* leads to changes in mDA neuron development *in vivo*, IUE with pLL3.7shcirc*Rmst* was performed on E12 vMB of *Pitx3*$^{Cre/WT}$ mouse embryos. At E18, mDA neurons had moved farther laterally from the midline in pLL3.7shcirc*Rmst* knockdown, compared to empty vector pLL3.7GFP control (unpublished data; not shown).

To see if the increase in soma size *in vitro* could be observed *in vivo* as well, soma size of *in utero* electroporated TH-positive neurons was measured. It was found that there is no significant difference between pLL3.7shcirc*Rmst* knockdown and empty vector pLL3.7GFP in *in utero* electroporated TH-positive neurons (Figure 3).

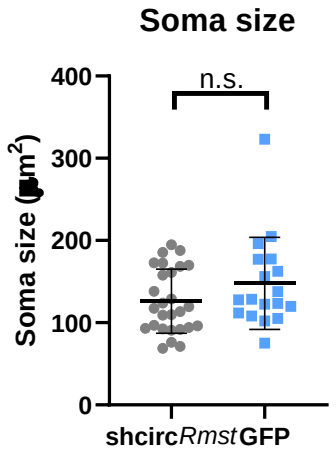

Figure 3. Soma size circRmst knockdown in utero electroporated neurons *Soma size was measured from in utero electroporated (E12-E18) vMB that received either pLL3.7GFP empty vector control or pLL3.7shcircRmst knockdown. There is no significant difference in soma size between circRmst knockdown and control. (not significant (n.s.); bars: mean ± S.E.).*

3.3 VTA is visualised in *Pitx3Flp:CCK-Cre:Ai65* E16 mouse brain after whole brain clearing using 3DISCO and IDISCO

Using quantitative polymerase chain reaction (qPCR) on micro-dissected and Fluorescence-activated Cell Sorting (FACS)-sorted VTA and SNc, it was shown that circ*Rmst* is primarily expressed in the VTA and not in the SNc during development (unpublished data; not shown). To visualise where the VTA is located in the developing mouse brain, *Pitx3Flp:CCK-Cre:Ai65* mice were used. Pitx3 is one of the earliest markers of mDA neurons and CCK marks the VTA in the vMB (Smidt et al., 1997; Veenvliet et al., 2013). Ai65 is a dual td-Tomato (TdT) reporter. Triple positive *Pitx3Flp:CCK-Cre:Ai65* mice only express TdT in cells that express both Pitx3-flp and CCK-cre, which means that TdT is very specifically expressed in mDA neurons of the VTA (Madisen et al., 2015; Taniguchi et al., 2011). To optimalise visualising the VTA in developing mouse brains, two different whole tissue clearing methods (3DISCO and iDISCO) were used. Both 3DISCO and iDISCO can be used to efficiently clear embryonic mouse brains, without quenching fluorescent proteins (Ertürk et al., 2012; Renier et al., 2014). E16 mouse brains were used as the VTA has already started forming at this age (Kawano et al., 1995). Lastly, it was tested if centrifuging both primary and secondary antibodies for 30 minutes at 130000 g before incubation results in less aspecific binding.

In 3DISCO cleared *Pitx3Flp:CCK-Cre:Ai65* E16 brains, stained with non-centrifuged antibodies, the mDA system could be seen clearly, as well as the VTA (Figure 4 (A)). In iDISCO cleared *Pitx3Flp:CCK-Cre:Ai65* E16 brains, the mDA system and the VTA could be seen clearly as well (Figure 4 (B,C)), but the resolution of images made of iDISCO cleared brains was higher than images made from 3DISCO cleared brains at the same magnification (Figure 4 (A-C)). Some aspecific binding of antibodies could be seen in both 3DISCO and iDISCO cleared brains without centrifuging of antibodies (Figure 4 (A1,B1)). Centrifuging of antibodies led to less aspecific binding of antibodies (Figure 4 (C)). Based on these results, we suggest using iDISCO combined with centrifuging of antibodies for staining and

clearing embryonic mice brains.

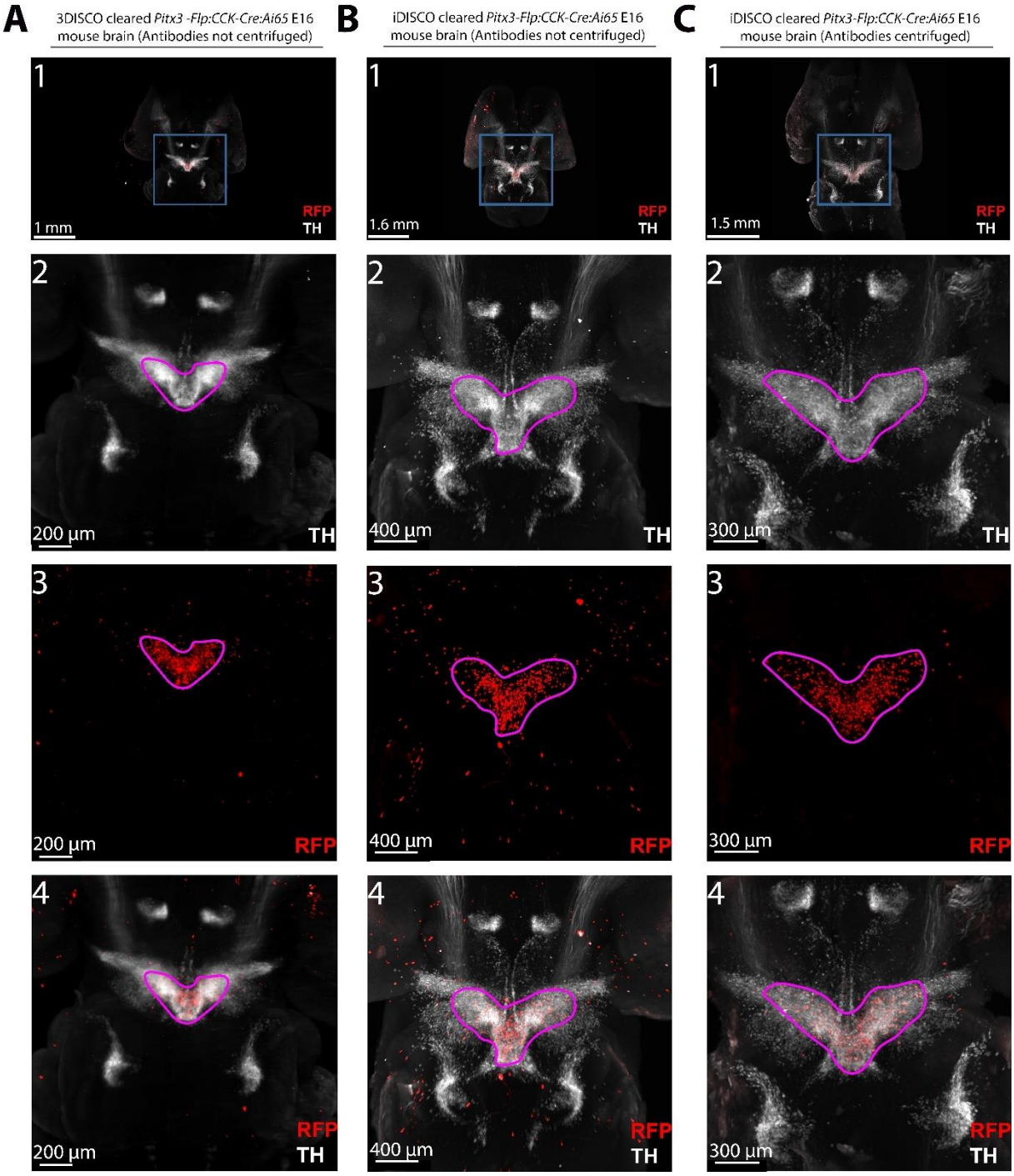

Figure 4. Visualising VTA in Pitx3Flp:CCK-Cre:Ai65 E16 mouse brains *VTA is visualised in Pitx3Flp:CCK-Cre:Ai65 E16 mouse brains by whole brain clearing using 3DISCO (A) and iDISCO (B,C). Brains are stained with anti-TH (mDA neurons) and anti-RFP (mDA neurons of VTA) antibodies. Anti-TH and anti-RFP antibodies are either not centrifuged (A,B) or centrifuged for 30 minutes at 130000 g (C). Whole brain is imaged (A1,B1,C1). VTA is marked with a magenta shape (A2-4,B2-4,C2-4).*

4. Discussion

4.1 Soma size and actin cytoskeleton

In this study we show that knockdown of circ*Rmst* leads to increased soma size and complexity of mDA neurons and a decrease of mDA neurons during development *in vitro*. It has also been shown before that circ*Rmst* knockdown leads to defects in mDA neuron position *in vivo* (unpublished data; not shown).

The question now arises, how does a knockdown of circ*Rmst* lead to an increase in soma size and neuron complexity *in vitro*? A clue may lie in the fact that somas of mDA neurons with a knockdown of circ*Rmst* have big lamellipodia. Lamellipodia are protrusions from the cell body, which are responsible for migration and neurite development (Mattila and Lappalainen, 2008). Lamellipodia are formed by polymerisation of actin filaments, which is mediated by the Actin Related Protein 2/3 (Arp2/3) complex (Wu et al., 2012). The Arp2/3 complex provides actin nucleation sites, leading to actin branching, which pushes the cell forward. The Wiskott–Aldrich syndrome protein (WASP) family and the WASP verprolin-homologous protein (WAVE) family are required for lamellipodia formation by activating the Arp2/3 complex (Takenawa and Miki, 2001). WASP/WAVE proteins form a complex together with Abelson-interacting protein 1 (Abi-1), which binds directly to hnRNPK (Proepper et al., 2011). *Rmst* binds directly to hnRNPK as well (Cheng et al., 2020). It is possible that circ*Rmst* also binds to hnRNPK, as the sequences of *Rmst* and circ*Rmst* are very similar. circ*Rmst* could act as a negative regulator of lamellipodia by occupying hnRNPK or having a direct interaction with the Abi-1/WASP/WAVE complex. Both options could lead to inhibition of the Abi-1/WASP/WAVE complex, which would decrease Arp2/3 and actin activity. Therefore, it should be studied if circ*Rmst* can bind to hnRNPK and if this interaction leads to inhibition of the Arp2/3 complex activity.

If circ*Rmst* regulates lamellipodia formation, we should expect more actin polymerisation in circ*Rmst* knockdown mDA neurons. To study if the actin cytoskeleton is upregulated in knockdown, actin can be stained with phalloidin in vMB primary cultures (Wulf et al., 1979). Furthermore, actin dynamics can be visualised as well using Lifeact (Riedl et al., 2008). Lifeact is a peptide that is able to stain filamentous actin (F-actin) in alive neurons (Riedl et al., 2008). Moreover, Lifeact does not interfere with actin dynamics. Because of this, dynamics of the actin cytoskeleton could be visualised in primary cultures of the vMB with a circ*Rmst* knockdown using live imaging.

4.2 Possible function in mDA neuron differentiation or survivability

Knockdown of circ*Rmst* in vMB primary cultures leads to a decrease in the amount of TH-positive neurons. The long non-coding isoform *Rmst*, is involved in neurogenesis and neuron differentiation (Ng et al., 2013). Furthermore, *Rmst* is also involved in mDA neuron defining pathways in combination with transcription factors such as Lmx1b and Wnt1, which are essential for mDA neuron survivability (Anderegg et al., 2013). In the beforementioned studies, the existence of circ*Rmst* was not yet known, therefore, the effects found in the studies may be partly caused by circ*Rmst*. Another study hinting at a role of circ*Rmst* in mDA neuron identity found that circ*Rmst* is upregulated in Wnt medullablastoma and can be used as a biomarker for this subtype (Rickert et al., 2021). This further suggests that circ*Rmst* is involved in mDA neuron defining pathways.

The reduction of the TH-positive neuron percentage found in circ*Rmst* knockdown could be explained by the inability of mDA neuron precursors to correctly generate and differentiate into mature mDA neurons. Knockdown of circ*Rmst* could also inhibit mDA neuron survivability. Both hypotheses would lead to a reduced amount of mDA neurons. To study whether mDA neuron progenitors become mature less or more slowly when circ*Rmst* is knocked down, a marker for mDA neuron progenitors such as Lmx1a could be used on E14 vMB primary cultures. If circ*Rmst* knockdown causes a slower maturation of mDA neuron progenitors, an increase in Lmx1a positive and TH-negative neurons compared to Scr2 control would be expected (Yan et al., 2011). To test if circ*Rmst* knockdown leads to increased mDA neuron death, cultures could be kept alive longer before fixation and staining. If circ*Rmst* is involved in mDA neuron survivability, the decrease in TH-positive cell percentage should be larger in circ*Rmst* knockdown compared to control when cultures are kept for a longer amount of time.

4.3 Relationship between soma size, percentage TH-positive cells and migration

Whereas *in vitro* an increase in soma size is seen, *in vivo* this phenotype is not found. One of the main reasons why there could be a difference between *in vivo* and *in vitro* is that *in vivo* cells have many different cell-cell interactions. Cells stick together using adhesion proteins and signalling molecules are interchanged between cells. *In vitro*, cells are much more separated from each other, meaning that other cells cannot influence each other as much.

A second explanation could be that neurons *in vitro* have much more space than *in vivo*. Cells are much more densely packed *in vivo*, which may make growing of the soma more difficult. Another factor that may influence the results is the fact that to determine soma size, surface area of a 2D picture of cells is measured. In culture, cells may be much flatter, whereas *in vivo* they may be more rounded. A way to counteract this problem may be to make images of primary cultures in Z-stacks and calculate volume instead of surface area. Volume of mDA neurons *in vivo* can also be determined using 3DISCO or iDISCO clearing, as these techniques allow 3D imaging of whole brains.

Even though no increase in soma size is found *in vivo*, an alteration in position of mDA neurons is found. mDA neurons normally first migrate radially from the ventricular zone through the mantle layer, after which they migrate tangentially to form the VTA and SNc (Figure 5; Blaess and Ang, 2015). mDA neurons end up more lateral in the vMB in the circ*Rmst* knockdown condition compared to empty vector control (unpublished data). This indicates that the tangential migration is defected in the circ*Rmst* knockdown condition. This change in position could be caused either by an increase in migration speed or cell death of slower migrating neurons.

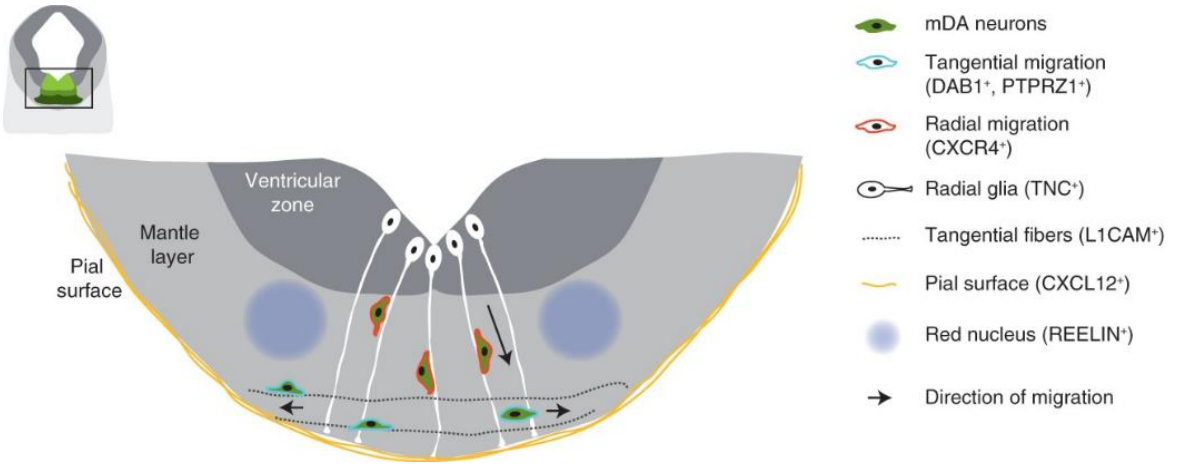

Figure 5. Schematic overview of migration of mDA neurons at E12.5 *Migration of mDA neurons starts at the ventricular zone from which they migrate radially along radial glia to the mantle layer. After reaching the mantle layer, mDA neurons migrate tangentially in the direction of the Pial surface to form the VTA and SNc (Modified from Blaess and Ang, 2015).*

As stated before, lamellipodia are actin based extensions from the soma, which are essential for neuronal migration (Mattila and Lappalainen, 2008). We find *in vitro* that a circ*Rmst* knockdown leads to increased soma size and neuron complexity, which could be due to enhanced lamellipodia formation. It is possible that knocking down circ*Rmst* leads to an increase in lamellipodia formation, which causes an increase in migration speed of mDA neurons.

The percentage of TH-positive neurons that are found in circ*Rmst* knockdown *in vitro* is decreased, possibly because circ*Rmst* is important for survival of mDA neurons. Furthermore, circ*Rmst* expression in the SNc is significantly less compared to the VTA (not shown). This means that the effect of the circ*Rmst* knockdown will be higher in VTA neurons compared to SNc neurons. Therefore, it is possible that *in vivo*, mDA neurons destined for the VTA tend to die quicker than neurons destined for the SNc when circ*Rmst* is silenced. Because SNc neurons have to migrate

further tangentially than VTA neurons, the effect of circ*Rmst* knockdown could be seen as a net increase in tangential migration.

To determine if one of these hypotheses is true, live imaging of cultured brain slices could be done (Ogaki et al., 2020). *Ex vivo* electroporation could be performed on dissected E12 brains with the same pLL3.7shcirc*Rmst* construct. Migrating mDA neurons could be followed to see if migration is sped up or if certain neurons die when circ*Rmst* is silenced.

4.4 mTOR signalling

Knockdown of circ*Rmst* led to an increase in soma size *in vitro*, possibly through a role in regulating the actin cytoskeleton. Interestingly, the mechanistic target of rapamycin (mTOR) pathway is involved in regulating the actin cytoskeleton and soma size (Angliker and Rüegg, 2013; Kwon et al., 2003). Lack of inhibitors of mTOR signalling, such as Phosphatase and tensin homolog (PTEN), Tuberous Sclerosis Complex 2 (TSC2) or Dep Domain Containing 5 (DEPDC5), led to an increase in soma size (Iffland et al., 2020; Weston et al., 2014). The same phenotype could be seen in overexpression of constitutively active mTOR stimulators Phosphoinositide 3-kinase (PI3K) and RAC-alpha serine/threonine-protein kinase (Akt1) (Kumar et al., 2005). Similarly, a decrease in soma size could be found if PI3K and Akt1 are inhibited (Kumar et al., 2005). Lastly, mTOR interacts with Arp2/3, leading to increased actin polymerisation (Zhao et al., 2021).

Knowing that mTOR signalling is a regulator of soma size, it can be hypothesized that circ*Rmst* is involved in the mTOR pathway as well. However, it has also been shown that activation of the mTOR pathway led to an increase in the amount of TH-positive neurons, which is in stark contrast to the decrease of TH-positive neurons found in circ*Rmst* knockdown (Diaz-Ruiz et al., 2009; Domanskyi et al., 2011). This means that if circ*Rmst* is part of the mTOR pathway, it would have to regulate TH survivability in another manner not related to the mTOR pathway. It is possible that circ*Rmst* is inhibited downstream of mTOR in a part of the pathway that is only responsible for the soma size increase.

It would be interesting to study if overexpression of circ*Rmst* leads to the same decrease in soma size as mTOR inhibition and increase in mDA neuron percentage. If this is the case, it could be investigated if the soma size decrease and mDA neuron percentage increase, induced by circ*Rmst* overexpression, would be rescued by overexpression of mTOR. If circ*Rmst* is inhibited downstream by mTOR, the phenotypes should be reversed. Actin cytoskeletal localisation and dynamics can also be studied comparing mTOR overexpression to circ*Rmst* knockdown. If circ*Rmst* is inhibited downstream by mTOR, cytoskeleton localisation and dynamics should be similar between conditions.

4.5 Whole brain clearing optimalisation

Whole *Pitx3Flp:CCK-Cre:Ai65* E16 brains were cleared using 3DISCO or iDISCO. iDISCO has the advantage that when clearing, the tissue does not shrink and that fluorescence is better conserved (Renier et al., 2014). In 3DISCO clearing the tissue can shrink up to half its original size depending on the tissue (Ertürk and Bradke, 2013). The shrinkage during 3DISCO clearing happens because of the use of THF and is not found in iDISCO because Methanol is used instead. Since the tissue shrinks in 3DISCO and the size does not change in iDISCO, the resolution of images that are taken from iDISCO cleared brains at the same magnification, will be higher than in 3DISCO cleared brains.

In 3DISCO and iDISCO the clearing will often have imperfections, which means that in larger tissues, it is harder for the light from the microscope to penetrate the entire piece of tissue. An advantage of 3DISCO can be that due to the shrinkage, the distance and tissue that the light has to travel through decreases. However, with small embryonic brains, even without shrinkage from 3DISCO, the light is strong enough to pass through the entire tissue. In accordance with the latter, we have found that,

for imaging E16 brains, iDISCO is the method that suits this tissue better. It needs to be tested if iDISCO is also is better for older embryonic ages and postnatal brains or if 3DISCO is prefered.

In iDISCO cleared brains, antibodies were either centrifuged at 130000 g for 30 mins or not. Centrifuging of antibodies led to much less aspecific binding of antibodies. It did so by removing antibody clumps, which can stick to aspecific locations in the brain. This means that, with our equipment, the best way to visualise the VTA in E16 brains is to centrifuge antibodies before incubation and to clear brains with iDISCO.

5. Conclusion

Development of the mDA system is a delicate process, requiring many transcription factors and growth factors to function together to lead to correct mDA system patterning and differentiation (Arenas et al., 2015). Errors in development can lead to severe neurological disorders such as schizophrenia or drug addiction (Bannon et al., 2002; Buervenich et al., 2000). Besides proteins that play a role in mDA neuron development, many ncRNAs are essential as well (Reviewed by Pascale et al., 2020). Because of the recent discovery that circRNAs have a spatiotemporal expression with an especially high expression in the developing brain, the role of circRNAs in mDA neurons was investigated (Rybak-Wolf et al., 2015; Venø et al., 2015).

In this study, we provide the first evidence that circ*Rmst* has a function in the development of mDA neurons. We show that knockdown of circ*Rmst in vitro* leads to increase in soma size and neuron complexity, which could suggest that circ*Rmst* has an effect on cytoskeleton structure. Furthermore, circ*Rmst* knockdown also leads to a decrease in TH-positive mDA neurons, indicating that circ*Rmst* may play a role in mDA neuron survivability. circ*Rmst* knockdown *in vivo* leads to an increased tangential position of mDA neurons, but not to an increased soma size. To unravel the molecular mechanisms of circ*Rmst*, future studies should focus on investigating cytoskeleton structure and dynamics, and mDA neuron differentiation and survivability pathways.

Acknowledgements

I thank Mateja Rybiczka-Tesulov for her awesome daily supervision and teaching me so many new things in the lab. I also thank Laurens Grossouw for being a great genotyping partner and helping me with the 3DISCO and iDISCO clearing. Lastly I thank prof. dr. R.J. Pasterkamp for letting me join a dedicated and fun lab.

Literature

Aktaş, T., Avşar Ilık, İ., Maticzka, D., Bhardwaj, V., Pessoa Rodrigues, C., Mittler, G., Manke, T., Backofen, R., Akhtar, A., 2017. DHX9 suppresses RNA processing defects originating from the Alu invasion of the human genome. Nature 544, 115–119. https://doi.org/10.1038/nature21715

Ambros, V., 2004. The functions of animal microRNAs. Nature 431, 350–355. https://doi.org/10.1038/nature02871

Anderegg, A., Lin, H.-P., Chen, J.-A., Caronia-Brown, G., Cherepanova, N., Yun, B., Joksimovic, M., Rock, J., Harfe, B.D., Johnson, R., Awatramani, R., 2013. An Lmx1b-miR135a2 Regulatory Circuit Modulates Wnt1/Wnt Signaling and Determines the Size of the Midbrain Dopaminergic Progenitor Pool. PLOS Genetics 9, e1003973. https://doi.org/10.1371/journal.pgen.1003973

Angliker, N., Rüegg, M.A., 2013. In vivo evidence for mTORC2-mediated actin cytoskeleton rearrangement in neurons. BioArchitecture 3, 113–118. https://doi.org/10.4161/bioa.26497

Arenas, E., Denham, M., Villaescusa, J.C., 2015. How to make a midbrain dopaminergic neuron. Development 142, 1918–1936. https://doi.org/10.1242/dev.097394

Ashwal-Fluss, R., Meyer, M., Pamudurti, N.R., Ivanov, A., Bartok, O., Hanan, M., Evantal, N., Memczak, S., Rajewsky, N., Kadener, S., 2014. circRNA Biogenesis Competes with Pre-mRNA Splicing. Molecular Cell 56, 55–66. https://doi.org/10.1016/j.molcel.2014.08.019

Bannon, M.J., Pruetz, B., Manning-Bog, A.B., Whitty, C.J., Michelhaugh, S.K., Sacchetti, P., Granneman, J.G., Mash, D.C., Schmidt, C.J., 2002. Decreased expression of the transcription factor NURR1 in dopamine neurons of cocaine abusers. Proc Natl Acad Sci U S A 99, 6382–6385. https://doi.org/10.1073/pnas.092654299

Birney, E., Stamatoyannopoulos, J.A., Dutta, A., Guigó, R., Gingeras, T.R., Margulies, E.H., Weng, Z., Snyder, M., Dermitzakis, E.T., Stamatoyannopoulos, J.A., Thurman, R.E., Kuehn, M.S., Taylor, C.M., Neph, S., Koch, C.M., Asthana, S., Malhotra, A., Adzhubei, I., Greenbaum, J.A., Andrews, R.M., Flicek, P., Boyle, P.J., Cao, H., Carter, N.P., Clelland, G.K., Davis, S., Day, N., Dhami, P., Dillon, S.C., Dorschner, M.O., Fiegler, H., Giresi, P.G., Goldy, J., Hawrylycz, M., Haydock, A., Humbert, R., James, K.D., Johnson, B.E., Johnson, E.M., Frum, T.T., Rosenzweig, E.R., Karnani, N., Lee, K., Lefebvre, G.C., Navas, P.A., Neri, F., Parker, S.C.J., Sabo, P.J., Sandstrom, R., Shafer, A., Vetrie, D., Weaver, M., Wilcox, S., Yu, M., Collins, F.S., Dekker, J., Lieb, J.D., Tullius, T.D., Crawford, G.E., Sunyaev, S., Noble, W.S., Dunham, I., Dutta, A., Guigó, R., Denoeud, F., Reymond, A., Kapranov, P., Rozowsky, J., Zheng, D., Castelo, R., Frankish, A., Harrow, J., Ghosh, S., Sandelin, A., Hofacker, I.L., Baertsch, R., Keefe, D., Flicek, P., Dike, S., Cheng, J., Hirsch, H.A., Sekinger, E.A., Lagarde, J., Abril, J.F., Shahab, A., Flamm, C., Fried, C., Hackermüller, J., Hertel, J., Lindemeyer, M., Missal, K., Tanzer, A., Washietl, S., Korbel, J., Emanuelsson, O., Pedersen, J.S., Holroyd, N., Taylor, R., Swarbreck, D., Matthews, N., Dickson, M.C., Thomas, D.J., Weirauch, M.T., Gilbert, J., Drenkow, J., Bell, I., Zhao, X., Srinivasan, K.G., Sung, W.-K., Ooi, H.S., Chiu, K.P., Foissac, S., Alioto, T., Brent, M., Pachter, L., Tress, M.L., Valencia, A., Choo, S.W., Choo, C.Y., Ucla, C., Manzano, C., Wyss, C., Cheung, E., Clark, T.G., Brown, J.B., Ganesh, M., Patel, S., Tammana, H., Chrast, J., Henrichsen, C.N., Kai, C., Kawai, J., Nagalakshmi, U., Wu, J., Lian, Z., Lian, J., Newburger, P., Zhang, X., Bickel, P., Mattick, J.S., Carninci, P., Hayashizaki, Y., Weissman, S., Dermitzakis, E.T., Margulies, E.H., Hubbard, T., Myers, R.M., Rogers, J., Stadler, P.F., Lowe, T.M., Wei, C.-L., Ruan, Y., Snyder, M., Birney, E., Struhl, K., Gerstein, M., Antonarakis, S.E., Gingeras, T.R., Brown, J.B., Flicek, P., Fu, Y., Keefe, D., Birney, E., Denoeud, F., Gerstein, M., Green, E.D., Kapranov, P., Karaöz, U., Myers, R.M., Noble, W.S., Reymond, A., Rozowsky, J., Struhl, K., Siepel, A., Stamatoyannopoulos, J.A., Taylor, C.M., Taylor, J., Thurman, R.E., Tullius, T.D., Washietl, S., Zheng, D., Liefer, L.A., Wetterstrand, K.A., Good, P.J., Feingold, E.A., Guyer, M.S., Collins, F.S., Margulies, E.H., Cooper, G.M., Asimenos, G., Thomas, D.J., Dewey, C.N., Siepel, A., Birney, E., Keefe, D., Hou, M., Taylor, J., Nikolaev, S., Montoya-Burgos, J.I., Löytynoja, A., Whelan, S.,

Pardi, F., Massingham, T., Brown, J.B., Huang, H., Zhang, N.R., Bickel, P., Holmes, I., Mullikin, J.C., Ureta-Vidal, A., Paten, B., Seringhaus, M., Church, D., Rosenbloom, K., Kent, W.J., Stone, E.A., Gerstein, M., Antonarakis, S.E., Batzoglou, S., Goldman, N., Hardison, R.C., Haussler, D., Miller, W., Pachter, L., Green, E.D., Sidow, A., Weng, Z., Trinklein, N.D., Fu, Y., Zhang, Z.D., Karaöz, U., Barrera, L., Stuart, R., Zheng, D., Ghosh, S., Flicek, P., King, D.C., Taylor, J., Ameur, A., Enroth, S., Bieda, M.C., Koch, C.M., Hirsch, H.A., Wei, C.-L., Cheng, J., Kim, J., Bhinge, A.A., Giresi, P.G., Jiang, N., Liu, J., Yao, F., Sung, W.-K., Chiu, K.P., Vega, V.B., Lee, C.W.H., Ng, P., Shahab, A., Sekinger, E.A., Yang, A., Moqtaderi, Z., Zhu, Z., Xu, X., Squazzo, S., Oberley, M.J., Inman, D., Singer, M.A., Richmond, T.A., Munn, K.J., Rada-Iglesias, A., Wallerman, O., Komorowski, J., Clelland, G.K., Wilcox, S., Dillon, S.C., Andrews, R.M., Fowler, J.C., Couttet, P., James, K.D., Lefebvre, G.C., Bruce, A.W., Dovey, O.M., Ellis, P.D., Dhami, P., Langford, C.F., Carter, N.P., Vetrie, D., Kapranov, P., The ENCODE Project Consortium, Analysis Coordination, Chromatin and Replication, Genes and Transcripts, Integrated Analysis and Manuscript Preparation, Management Group, Multi-species Sequence Analysis, NISC Comparative Sequencing Program*, Baylor College of Medicine Human Genome Sequencing Center*, Washington University Genome Sequencing Center*, Broad Institute*, Children's Hospital Oakland Research Institute*, Transcriptional Regulatory Elements, 2007. Identification and analysis of functional elements in 1% of the human genome by the ENCODE pilot project. Nature 447, 799–816. https://doi.org/10.1038/nature05874

Blaess, S., Ang, S.-L., 2015. Genetic control of midbrain dopaminergic neuron development. WIREs Developmental Biology 4, 113–134. https://doi.org/10.1002/wdev.169

Brown, A., Machan, J.T., Hayes, L., Zervas, M., 2011. Molecular organization and timing of Wnt1 expression define cohorts of midbrain dopamine neuron progenitors in vivo. Journal of Comparative Neurology 519, 2978–3000. https://doi.org/10.1002/cne.22710

Buervenich, S., Carmine, A., Arvidsson, M., Xiang, F., Zhang, Z., Sydow, O., Jönsson, E.G., Sedvall, G.C., Leonard, S., Ross, R.G., Freedman, R., Chowdari, K.V., Nimgaonkar, V.L., Perlmann, T., Anvret, M., Olson, L., 2000. NURR1 mutations in cases of schizophrenia and manic-depressive disorder. Am J Med Genet 96, 808–813. https://doi.org/10.1002/1096-8628(20001204)96:6<808::aid-ajmg23>3.0.co;2-e

Burdon, R.H., 1971. Ribonucleic Acid Maturation in animal Cells, in: Davidson, J.N., Cohn, W.E. (Eds.), Progress in Nucleic Acid Research and Molecular Biology. Academic Press, pp. 33–79. https://doi.org/10.1016/S0079-6603(08)60325-6

Capel, B., Swain, A., Nicolis, S., Hacker, A., Walter, M., Koopman, P., Goodfellow, P., Lovell-Badge, R., 1993. Circular transcripts of the testis-determining gene Sry in adult mouse testis. Cell 73, 1019–1030. https://doi.org/10.1016/0092-8674(93)90279-Y

Cech, T.R., 1990. Nobel lecture. Self-splicing and enzymatic activity of an intervening sequence RNA from Tetrahymena. Biosci Rep 10, 239–261. https://doi.org/10.1007/BF01117241

Chen, L.-L., Yang, L., 2015. Regulation of circRNA biogenesis. RNA Biology 12, 381–388. https://doi.org/10.1080/15476286.2015.1020271

Cheng, H., Sun, M., Wang, Z.-L., Wu, Q., Yao, J., Ren, G., Sun, X.-L., 2020. LncRNA RMST-mediated miR-107 transcription promotes OGD-induced neuronal apoptosis via interacting with hnRNPK. Neurochemistry International 133, 104644. https://doi.org/10.1016/j.neuint.2019.104644

Chung, S., Leung, A., Han, B.-S., Chang, M.-Y., Moon, J.-I., Kim, C.-H., Hong, S., Pruszak, J., Isacson, O., Kim, K.-S., 2009. Wnt1-lmx1a Forms a Novel Autoregulatory Loop and Controls Midbrain Dopaminergic Differentiation Synergistically with the SHH-FoxA2 Pathway. Cell Stem Cell 5, 646–658. https://doi.org/10.1016/j.stem.2009.09.015

Cocquerelle, C., Mascrez, B., Hétuin, D., Bailleul, B., 1993. Mis-splicing yields circular RNA molecules. The FASEB Journal 7, 155–160. https://doi.org/10.1096/fasebj.7.1.7678559

Conn, S.J., Pillman, K.A., Toubia, J., Conn, V.M., Salmanidis, M., Phillips, C.A., Roslan, S., Schreiber, A.W., Gregory, P.A., Goodall, G.J., 2015. The RNA Binding Protein Quaking Regulates Formation of circRNAs. Cell 160, 1125–1134. https://doi.org/10.1016/j.cell.2015.02.014

Deng, Q., Andersson, E., Hedlund, E., Alekseenko, Z., Coppola, E., Panman, L., Millonig, J.H., Brunet, J.-F., Ericson, J., Perlmann, T., 2011. Specific and integrated roles of Lmx1a, Lmx1b and Phox2a in ventral midbrain development. Development 138, 3399–3408. https://doi.org/10.1242/dev.065482

Diaz-Ruiz, O., Zapata, A., Shan, L., Zhang, Y., Tomac, A.C., Malik, N., de la Cruz, F., Bäckman, C.M., 2009. Selective deletion of PTEN in dopamine neurons leads to trophic effects and adaptation of striatal medium spiny projecting neurons. PLoS One 4, e7027. https://doi.org/10.1371/journal.pone.0007027

Domanskyi, A., Geissler, C., Vinnikov, I.A., Alter, H., Schober, A., Vogt, M.A., Gass, P., Parlato, R., Schütz, G., 2011. Pten ablation in adult dopaminergic neurons is neuroprotective in Parkinson's disease models. FASEB J 25, 2898–2910. https://doi.org/10.1096/fj.11-181958

Du, W.W., Yang, W., Liu, E., Yang, Z., Dhaliwal, P., Yang, B.B., 2016. Foxo3 circular RNA retards cell cycle progression via forming ternary complexes with p21 and CDK2. Nucleic Acids Res 44, 2846–2858. https://doi.org/10.1093/nar/gkw027

Elgar, G., Vavouri, T., 2008. Tuning in to the signals: noncoding sequence conservation in vertebrate genomes. Trends in Genetics 24, 344–352. https://doi.org/10.1016/j.tig.2008.04.005

Errichelli, L., Dini Modigliani, S., Laneve, P., Colantoni, A., Legnini, I., Capauto, D., Rosa, A., De Santis, R., Scarfò, R., Peruzzi, G., Lu, L., Caffarelli, E., Shneider, N.A., Morlando, M., Bozzoni, I., 2017. FUS affects circular RNA expression in murine embryonic stem cell-derived motor neurons. Nat Commun 8, 14741. https://doi.org/10.1038/ncomms14741

Ertürk, A., Becker, K., Jährling, N., Mauch, C.P., Hojer, C.D., Egen, J.G., Hellal, F., Bradke, F., Sheng, M., Dodt, H.-U., 2012. Three-dimensional imaging of solvent-cleared organs using 3DISCO. Nat Protoc 7, 1983–1995. https://doi.org/10.1038/nprot.2012.119

Ertürk, A., Bradke, F., 2013. High-resolution imaging of entire organs by 3-dimensional imaging of solvent cleared organs (3DISCO). Experimental Neurology, New imaging techniques 242, 57–64. https://doi.org/10.1016/j.expneurol.2012.10.018

Hansen, T.B., Jensen, T.I., Clausen, B.H., Bramsen, J.B., Finsen, B., Damgaard, C.K., Kjems, J., 2013. Natural RNA circles function as efficient microRNA sponges. Nature 495, 384–388. https://doi.org/10.1038/nature11993

Hsu, M.-T., Coca-Prados, M., 1979. Electron microscopic evidence for the circular form of RNA in the cytoplasm of eukaryotic cells. Nature 280, 339–340. https://doi.org/10.1038/280339a0

Iffland, P.H., Barnes, A.E., Baybis, M., Crino, P.B., 2020. Dynamic analysis of 4E-BP1 phosphorylation in neurons with Tsc2 or Depdc5 knockout. Experimental Neurology 334, 113432. https://doi.org/10.1016/j.expneurol.2020.113432

Ivanov, A., Memczak, S., Wyler, E., Torti, F., Porath, H.T., Orejuela, M.R., Piechotta, M., Levanon, E.Y., Landthaler, M., Dieterich, C., Rajewsky, N., 2015. Analysis of Intron Sequences Reveals Hallmarks of Circular RNA Biogenesis in Animals. Cell Reports 10, 170–177. https://doi.org/10.1016/j.celrep.2014.12.019

Izuogu, O.G., Alhasan, A.A., Mellough, C., Collin, J., Gallon, R., Hyslop, J., Mastrorosa, F.K., Ehrmann, I., Lako, M., Elliott, D.J., Santibanez-Koref, M., Jackson, M.S., 2018. Analysis of human ES cell differentiation establishes that the dominant isoforms of the lncRNAs RMST and FIRRE are circular. BMC Genomics 19, 276. https://doi.org/10.1186/s12864-018-4660-7

Jeck, W.R., Sorrentino, J.A., Wang, K., Slevin, M.K., Burd, C.E., Liu, J., Marzluff, W.F., Sharpless, N.E., 2013. Circular RNAs are abundant, conserved, and associated with ALU repeats. RNA 19, 141–157. https://doi.org/10.1261/rna.035667.112

Kawano, H., Ohyama, K., Kawamura, K., Nagatsu, I., 1995. Migration of dopaminergic neurons in the embryonic mesencephalon of mice. Developmental Brain Research 86, 101–113. https://doi.org/10.1016/0165-3806(95)00018-9

Koh, H.R., Xing, L., Kleiman, L., Myong, S., 2014. Repetitive RNA unwinding by RNA helicase A facilitates RNA annealing. Nucleic Acids Research 42, 8556–8564. https://doi.org/10.1093/nar/gku523

Kruger, K., Grabowski, P.J., Zaug, A.J., Sands, J., Gottschling, D.E., Cech, T.R., 1982. Self-splicing RNA: Autoexcision and autocyclization of the ribosomal RNA intervening sequence of tetrahymena. Cell 31, 147–157. https://doi.org/10.1016/0092-8674(82)90414-7

Kumar, V., Zhang, M.-X., Swank, M.W., Kunz, J., Wu, G.-Y., 2005. Regulation of Dendritic Morphogenesis by Ras–PI3K–Akt–mTOR and Ras–MAPK Signaling Pathways. J. Neurosci. 25, 11288–11299. https://doi.org/10.1523/JNEUROSCI.2284-05.2005

Kwon, C.-H., Zhu, X., Zhang, J., Baker, S.J., 2003. mTor is required for hypertrophy of Pten-deficient neuronal soma in vivo. Proc Natl Acad Sci U S A 100, 12923–12928. https://doi.org/10.1073/pnas.2132711100

Li, X., Liu, C.-X., Xue, W., Zhang, Y., Jiang, S., Yin, Q.-F., Wei, J., Yao, R.-W., Yang, L., Chen, L.-L., 2017. Coordinated circRNA Biogenesis and Function with NF90/NF110 in Viral Infection. Molecular Cell 67, 214-227.e7. https://doi.org/10.1016/j.molcel.2017.05.023

Li, Z., Huang, C., Bao, C., Chen, L., Lin, M., Wang, X., Zhong, G., Yu, B., Hu, W., Dai, L., Zhu, P., Chang, Z., Wu, Q., Zhao, Y., Jia, Y., Xu, P., Liu, H., Shan, G., 2015. Exon-intron circular RNAs regulate transcription in the nucleus. Nat Struct Mol Biol 22, 256–264. https://doi.org/10.1038/nsmb.2959

Liang, D., Tatomer, D.C., Luo, Z., Wu, H., Yang, L., Chen, L.-L., Cherry, S., Wilusz, J.E., 2017. The Output of Protein-Coding Genes Shifts to Circular RNAs When the Pre-mRNA Processing Machinery Is Limiting. Molecular Cell 68, 940-954.e3. https://doi.org/10.1016/j.molcel.2017.10.034

Maass, P.G., Glažar, P., Memczak, S., Dittmar, G., Hollfinger, I., Schreyer, L., Sauer, A.V., Toka, O., Aiuti, A., Luft, F.C., Rajewsky, N., 2017. A map of human circular RNAs in clinically relevant tissues. J Mol Med 95, 1179–1189. https://doi.org/10.1007/s00109-017-1582-9

Madisen, L., Garner, A.R., Shimaoka, D., Chuong, A.S., Klapoetke, N.C., Li, L., van der Bourg, A., Niino, Y., Egolf, L., Monetti, C., Gu, H., Mills, M., Cheng, A., Tasic, B., Nguyen, T.N., Sunkin, S.M., Benucci, A., Nagy, A., Miyawaki, A., Helmchen, F., Empson, R.M., Knöpfel, T., Boyden, E.S., Reid, R.C., Carandini, M., Zeng, H., 2015. Transgenic mice for intersectional targeting of neural sensors and effectors with high specificity and performance. Neuron 85, 942–958. https://doi.org/10.1016/j.neuron.2015.02.022

Mattila, P.K., Lappalainen, P., 2008. Filopodia: molecular architecture and cellular functions. Nat Rev Mol Cell Biol 9, 446–454. https://doi.org/10.1038/nrm2406

Memczak, S., Jens, M., Elefsinioti, A., Torti, F., Krueger, J., Rybak, A., Maier, L., Mackowiak, S.D., Gregersen, L.H., Munschauer, M., Loewer, A., Ziebold, U., Landthaler, M., Kocks, C., le Noble, F., Rajewsky, N., 2013. Circular RNAs are a large class of animal RNAs with regulatory potency. Nature 495, 333–338. https://doi.org/10.1038/nature11928

Ng, S.-Y., Bogu, G.K., Soh, B.S., Stanton, L.W., 2013. The long noncoding RNA RMST interacts with SOX2 to regulate neurogenesis. Mol Cell 51, 349–359. https://doi.org/10.1016/j.molcel.2013.07.017

Ogaki, A., Araki, T., Ishikawa, M., Ikegaya, Y., Koyama, R., 2020. A live imaging-friendly slice culture method using collagen membranes. Neuropsychopharmacol Rep 40, 307–313. https://doi.org/10.1002/npr2.12128

Ono, Y., Nakatani, T., Sakamoto, Y., Mizuhara, E., Minaki, Y., Kumai, M., Hamaguchi, A., Nishimura, M., Inoue, Y., Hayashi, H., Takahashi, J., Imai, T., 2007. Differences in neurogenic potential in floor plate cells along an anteroposterior location: midbrain dopaminergic neurons originate from mesencephalic floor plate cells. Development 134, 3213–3225. https://doi.org/10.1242/dev.02879

Pamudurti, N.R., Bartok, O., Jens, M., Ashwal-Fluss, R., Stottmeister, C., Ruhe, L., Hanan, M., Wyler, E., Perez-Hernandez, D., Ramberger, E., Shenzis, S., Samson, M., Dittmar, G., Landthaler, M., Chekulaeva, M., Rajewsky, N., Kadener, S., 2017. Translation of CircRNAs. Molecular Cell 66, 9-21.e7. https://doi.org/10.1016/j.molcel.2017.02.021

Pascale, E., Divisato, G., Palladino, R., Auriemma, M., Ngalya, E.F., Caiazzo, M., 2020. Noncoding RNAs and Midbrain DA Neurons: Novel Molecular Mechanisms and Therapeutic Targets in Health and Disease. Biomolecules 10, 1269. https://doi.org/10.3390/biom10091269

Proepper, C., Steinestel, K., Schmeisser, M.J., Heinrich, J., Steinestel, J., Bockmann, J., Liebau, S., Boeckers, T.M., 2011. Heterogeneous Nuclear Ribonucleoprotein K Interacts with Abi-1 at Postsynaptic Sites and Modulates Dendritic Spine Morphology. PLoS One 6, e27045. https://doi.org/10.1371/journal.pone.0027045

Renier, N., Wu, Z., Simon, D.J., Yang, J., Ariel, P., Tessier-Lavigne, M., 2014. iDISCO: A Simple, Rapid Method to Immunolabel Large Tissue Samples for Volume Imaging. Cell 159, 896–910. https://doi.org/10.1016/j.cell.2014.10.010

Rhinn, M., Brand, M., 2001. The midbrain--hindbrain boundary organizer. Curr Opin Neurobiol 11, 34–42. https://doi.org/10.1016/s0959-4388(00)00171-9

Rickert, D., Bartl, J., Picard, D., Bernardi, F., Qin, N., Lovino, M., Puget, S., Meyer, F.-D., Mahoungou Koumba, I., Beez, T., Varlet, P., Dufour, C., Fischer, U., Borkhardt, A., Reifenberger, G., Ayrault, O., Remke, M., 2021. Circular RNA profiling distinguishes medulloblastoma groups and shows aberrant RMST overexpression in WNT medulloblastoma. Acta Neuropathol 141, 975–978. https://doi.org/10.1007/s00401-021-02306-2

Riedl, J., Crevenna, A.H., Kessenbrock, K., Yu, J.H., Neukirchen, D., Bista, M., Bradke, F., Jenne, D., Holak, T.A., Werb, Z., Sixt, M., Wedlich-Soldner, R., 2008. Lifeact: a versatile marker to visualize F-actin. Nat Methods 5, 605–607. https://doi.org/10.1038/nmeth.1220

Rybak-Wolf, A., Stottmeister, C., Glažar, P., Jens, M., Pino, N., Giusti, S., Hanan, M., Behm, M., Bartok, O., Ashwal-Fluss, R., Herzog, M., Schreyer, L., Papavasileiou, P., Ivanov, A., Öhman, M., Refojo, D., Kadener, S., Rajewsky, N., 2015. Circular RNAs in the Mammalian Brain Are Highly Abundant, Conserved, and Dynamically Expressed. Molecular Cell 58, 870–885. https://doi.org/10.1016/j.molcel.2015.03.027

Salzman, J., Chen, R.E., Olsen, M.N., Wang, P.L., Brown, P.O., 2013. Cell-Type Specific Features of Circular RNA Expression. PLOS Genetics 9, e1003777. https://doi.org/10.1371/journal.pgen.1003777

Salzman, J., Gawad, C., Wang, P.L., Lacayo, N., Brown, P.O., 2012. Circular RNAs Are the Predominant Transcript Isoform from Hundreds of Human Genes in Diverse Cell Types. PLOS ONE 7, e30733. https://doi.org/10.1371/journal.pone.0030733

Saucedo-Cardenas, O., Quintana-Hau, J.D., Le, W.-D., Smidt, M.P., Cox, J.J., De Mayo, F., Burbach, J.P.H., Conneely, O.M., 1998. Nurr1 is essential for the induction of the dopaminergic phenotype and the survival of ventral mesencephalic late dopaminergic precursor neurons. Proc Natl Acad Sci U S A 95, 4013–4018.

Smidt, M.P., Asbreuk, C.H.J., Cox, J.J., Chen, H., Johnson, R.L., Burbach, J.P.H., 2000. A second independent pathway for development of mesencephalic dopaminergic neurons requires Lmx1b. Nat Neurosci 3, 337–341. https://doi.org/10.1038/73902

Smidt, M.P., Schaick, H.S.A. van, Lanctôt, C., Tremblay, J.J., Cox, J.J., Kleij, A.A.M. van der, Wolterink, G., Drouin, J., Burbach, J.P.H., 1997. A homeodomain gene Ptx3 has highly restricted brain expression in mesencephalic dopaminergic neurons. PNAS 94, 13305–13310. https://doi.org/10.1073/pnas.94.24.13305

Smidt, M.P., von Oerthel, L., Hoekstra, E.J., Schellevis, R.D., Hoekman, M.F.M., 2012. Spatial and Temporal Lineage Analysis of a Pitx3-Driven Cre-Recombinase Knock-In Mouse Model. PLoS One 7, e42641. https://doi.org/10.1371/journal.pone.0042641

Starke, S., Jost, I., Rossbach, O., Schneider, T., Schreiner, S., Hung, L.-H., Bindereif, A., 2015. Exon Circularization Requires Canonical Splice Signals. Cell Reports 10, 103–111. https://doi.org/10.1016/j.celrep.2014.12.002

Takenawa, T., Miki, H., 2001. WASP and WAVE family proteins: key molecules for rapid rearrangement of cortical actin filaments and cell movement. J Cell Sci 114, 1801–1809.

Taniguchi, H., He, M., Wu, P., Kim, S., Paik, R., Sugino, K., Kvitsani, D., Fu, Y., Lu, J., Lin, Y., Miyoshi, G., Shima, Y., Fishell, G., Nelson, S.B., Huang, Z.J., 2011. A Resource of Cre Driver Lines for Genetic Targeting of GABAergic Neurons in Cerebral Cortex. Neuron 71, 995–1013. https://doi.org/10.1016/j.neuron.2011.07.026

Toulouse, A., Sullivan, A.M., 2008. Progress in Parkinson's disease—Where do we stand? Progress in Neurobiology 85, 376–392. https://doi.org/10.1016/j.pneurobio.2008.05.003

Tzschentke, T.M., Schmidt, W.J., 2000. Functional Relationship Among Medial Prefrontal Cortex, Nucleus Accumbens, and Ventral Tegmental Area in Locomotion and Reward. CRN 14. https://doi.org/10.1615/CritRevNeurobiol.v14.i2.20

Uhde, C.W., Vives, J., Jaeger, I., Li, M., 2010. Rmst Is a Novel Marker for the Mouse Ventral Mesencephalic Floor Plate and the Anterior Dorsal Midline Cells. PLOS ONE 5, e8641. https://doi.org/10.1371/journal.pone.0008641

Veenvliet, J.V., dos Santos, M.T.M.A., Kouwenhoven, W.M., von Oerthel, L., Lim, J.L., van der Linden, A.J.A., Koerkamp, M.J.A.G., Holstege, F.C.P., Smidt, M.P., 2013. Specification of dopaminergic subsets involves interplay of En1 and Pitx3. Development 140, 3373–3384. https://doi.org/10.1242/dev.094565

Venø, M.T., Hansen, T.B., Venø, S.T., Clausen, B.H., Grebing, M., Finsen, B., Holm, I.E., Kjems, J., 2015. Spatio-temporal regulation of circular RNA expression during porcine embryonic brain development. Genome Biology 16, 245. https://doi.org/10.1186/s13059-015-0801-3

Wang, P.L., Bao, Y., Yee, M.-C., Barrett, S.P., Hogan, G.J., Olsen, M.N., Dinneny, J.R., Brown, P.O., Salzman, J., 2014. Circular RNA Is Expressed across the Eukaryotic Tree of Life. PLOS ONE 9, e90859. https://doi.org/10.1371/journal.pone.0090859

Weston, M.C., Chen, H., Swann, J.W., 2014. Loss of mTOR repressors Tsc1 or Pten has divergent effects on excitatory and inhibitory synaptic transmission in single hippocampal neuron cultures. Front Mol Neurosci 7, 1. https://doi.org/10.3389/fnmol.2014.00001

Wu, C., Asokan, S.B., Berginski, M.E., Haynes, E.M., Sharpless, N.E., Griffith, J.D., Gomez, S.M., Bear, J.E., 2012. Arp2/3 complex is critical for lamellipodia and organization of cell-matrix adhesion but dispensable for fibroblast chemotaxis. Cell 148, 973–987. https://doi.org/10.1016/j.cell.2011.12.034

Wulf, E., Deboben, A., Bautz, F.A., Faulstich, H., Wieland, T., 1979. Fluorescent phallotoxin, a tool for the visualization of cellular actin. PNAS 76, 4498–4502. https://doi.org/10.1073/pnas.76.9.4498

Xia, S., Feng, J., Lei, L., Hu, J., Xia, L., Wang, J., Xiang, Y., Liu, L., Zhong, S., Han, L., He, C., 2017. Comprehensive characterization of tissue-specific circular RNAs in the human and mouse genomes. Briefings in Bioinformatics 18, 984–992. https://doi.org/10.1093/bib/bbw081

Yan, C.H., Levesque, M., Claxton, S., Johnson, R.L., Ang, S.-L., 2011. Lmx1a and lmx1b function cooperatively to regulate proliferation, specification, and differentiation of midbrain dopaminergic progenitors. J Neurosci 31, 12413–12425. https://doi.org/10.1523/JNEUROSCI.1077-11.2011

Zeng, Y., Du, W.W., Wu, Y., Yang, Z., Awan, F.M., Li, X., Yang, W., Zhang, C., Yang, Q., Yee, A., Chen, Y., Yang, F., Sun, H., Huang, R., Yee, A.J., Li, R.-K., Wu, Z., Backx, P.H., Yang, B.B., 2017. A Circular RNA Binds To and Activates AKT Phosphorylation and Nuclear Localization Reducing Apoptosis and Enhancing Cardiac Repair. Theranostics 7, 3842–3855. https://doi.org/10.7150/thno.19764

Zhang, X.-O., Wang, H.-B., Zhang, Y., Lu, X., Chen, L.-L., Yang, L., 2014. Complementary Sequence-Mediated Exon Circularization. Cell 159, 134–147. https://doi.org/10.1016/j.cell.2014.09.001

Zhao, Y., Schoeps, B., Yao, D., Zhang, Z., Schuck, K., Tissen, V., Jäger, C., Schlitter, A.M., van der Kammen, R., Ludwig, C., D'Haese, J.G., Raulefs, S., Maeritz, N., Shen, S., Zou, X., Krüger, A., Kleeff, J., Michalski, C.W., Friess, H., Innocenti, M., Kong, B., 2021. mTORC1 and mTORC2 Converge on the Arp2/3 Complex to Promote KrasG12D-Induced Acinar-to-Ductal Metaplasia and Early Pancreatic Carcinogenesis. Gastroenterology 160, 1755-1770.e17. https://doi.org/10.1053/j.gastro.2020.12.061